Title: Electrophysiologically-defined excitation-inhibition autism neurosubtypes

Authors: Natasha Bertelsen[1,2], Andrea Vitale[1], Dimitris Bolis[1], Veronica Mandelli[1,2], & Michael V. Lombardo[1]

Affiliations:

1 Laboratory for Autism and Neurodevelopmental Disorders, Center for Neuroscience and Cognitive Systems @UniTn, Istituto Italiano di Tecnologia, Rovereto, Italy

2 Center for Mind/Brain Sciences, University of Trento, Rovereto, Italy

Corresponding authors: Michael V. Lombardo (michael.lombardo@iit.it)

Abstract

Excitation-inhibition (E:I) imbalance has long been considered one of the primary neurobiological theories explaining autism. However, the theory has been bolstered heavily by research on high-penetrance genetic mechanisms which are only found in a small proportion of the autism population. Thus, how well does E:I imbalance explain idiopathic autism? Here we find that idiopathic autistic males can be split into two distinct E:I-defined 'neurosubtypes'. These E:I neurosubtypes can be identified in EEG data via an E:I-sensitive metric known as the Hurst exponent (H). Half of autistic individuals fall into the first E:I neurosubtype and can be described as having elevated E:I ratio relative to typically-developing (TD) comparison group. The remaining other half of autistic males fall into a second E:I neurosubtype with the opposite pattern of reduced E:I ratio relative to TD. Finally, E:I neurosubtypes show differential relationships between H and behavioral and demographic variables consisting of age, intelligence, and autism symptomatology. This work suggests that different types of E:I imbalance can manifest in idiopathic autistic males. Such differential E:I biomarkers may be indicative of distinctive etiological or compensatory mechanisms and differential underlying micro- and macroscale neural organization with differential phenotypic impact.

Imbalance between neurophysiological excitation and inhibition (henceforth referred to as 'E:I' imbalance) has long been considered one of the primary important neurobiological explanations behind autism[1]. While the theory has had impact on the field, it is notable that the theory rests on evidence primarily gleaned from animal model research on known high-impact genomic mechanisms linked to autism[2,3]. Nearly all of these genomic causes are rare in frequency, both within the general population but also within autism[4]. Evidence is limited that bridges the gap between such rare genomic mechanisms and more generalizable E:I explanations behind autistic individuals whose genetic etiologies are otherwise unknown (i.e. idiopathic autism). Sohal and Rubenstein[3] noted that the next steps in moving forward are towards identifying individualized biomarkers of different types of E:I imbalance which might lead towards differential explanations behind heterogeneity in behavioral phenotypes and/or differential responses to treatment.

In this work we examine EEG-derived biomarkers of different types of E:I balance in males with an otherwise idiopathic autism diagnosis. In prior work we have identified with in-silico computational and subsequent experimental animal model validation, that a statistical descriptor of aperiodic signal variation in neural time-series data known as the Hurst exponent (H), is an in-vivo biomarker sensitive to underlying synaptic E:I ratio[5]. Here we estimated H across the entire scalp with EEG in a relatively large (n=286) male idiopathic autism sample. We then utilized state-of-the-art relative clustering validation approaches[6] that allow us to identify in a data-driven manner discrete E:I 'neurosubtypes'[7]. Our approach also allows such data-driven insights to be immediately translated into a supervised classification model which we can test in new independent data for very high generalizability accuracy. The identified autism E:I 'neurosubtypes' are highly generalizable stratifications in the population and can be described as opposing types of E:I imbalance relative to the typically-developing (TD) comparison population. Individualized variability in E:I imbalance also relates to behavioral phenotypic variability in IQ and autism symptomatology in neurosubtype-specific manner. Overall, this work steps into the next phase of E:I research on autism[3] by unveiling that robust, yet opposing E:I neurosubtypes exist in autistic males and that each may provide differential explanations behind heterogeneous behavioral phenotypic variation in individuals whose genetic etiology is otherwise unknown (i.e. idiopathic).

Results

Identifying autism E:I neurosubtypes

We first set out to test whether E:I-sensitive EEG biomarkers such as H could be a meaningful neural stratifier of male idiopathic autistic individuals. We therefore applied unsupervised stability-based relative clustering validation analysis (*reval*)[6] to a relatively large EEG dataset of male autistic individuals (n=286) 5-21 years of age from data releases 1-10 from the Child Mind Institute Healthy Brain Network (CMI-HBN) dataset[8]. Genetic data was not available for analysis on this sample, and thus our usage of the term 'idiopathic' refers to the lack of knowledge regarding known genetic causes of autism. EEG data was examined under the two resting state conditions - eyes open and eyes closed. H was estimated across 93 electrodes across the scalp and then input into the *reval* clustering pipeline.

For both eyes open and eyes closed conditions, we find that the optimal number of subtypes is 2 (Figure 1A-B). Generalization accuracy for this 2-subtype solution in the held-out validation set is 92% for the resting state eyes open condition and 98% in the resting state eyes closed condition. This 2-cluster solution is indicative of true clusters, as it heavily deviates from a single multivariate Gaussian null distribution (SigClust analysis: all $p < 0.0015$ in training and validation sets for eyes open and eyes closed) (see Supplementary Table 1). Plots of dimensionality-reduced data with UMAP further show visually how the subtypes each have their own distribution and distinct peaks (Figure 1A-B). Thus, using EEG H patterns across the entire scalp, unsupervised data-driven clustering can robustly and replicably identify autism E:I 'neurosubtypes' that generalize with high-accuracy in new unseen datasets. These findings solidify the idea that at the very least, autism can be split into at least two E:I-defined neurosubtypes based on EEG biomarkers such as H.

In terms of the proportion of individuals within each subtype, we find that these E:I neurosubtypes comprise an approximate half-split of the entire autism sample examined (eyes open: autism subtype 1 = 45.45%, autism subtype 2 = 54.55%; eyes closed: autism subtype 1 = 52.10%, autism subtype 2 = 47.90%). A vast majority (n = 211; 73.78%) of participants are clustered into the same subtype across the two eye conditions (Figure 1C). The smaller subset of participants who changed subtypes between eyes open and eyes closed (n = 75; 26.22%), were not different from those that stayed in the same subtype in terms of age, FIQ, or autism symptomatology measures (Supplementary Table 2).

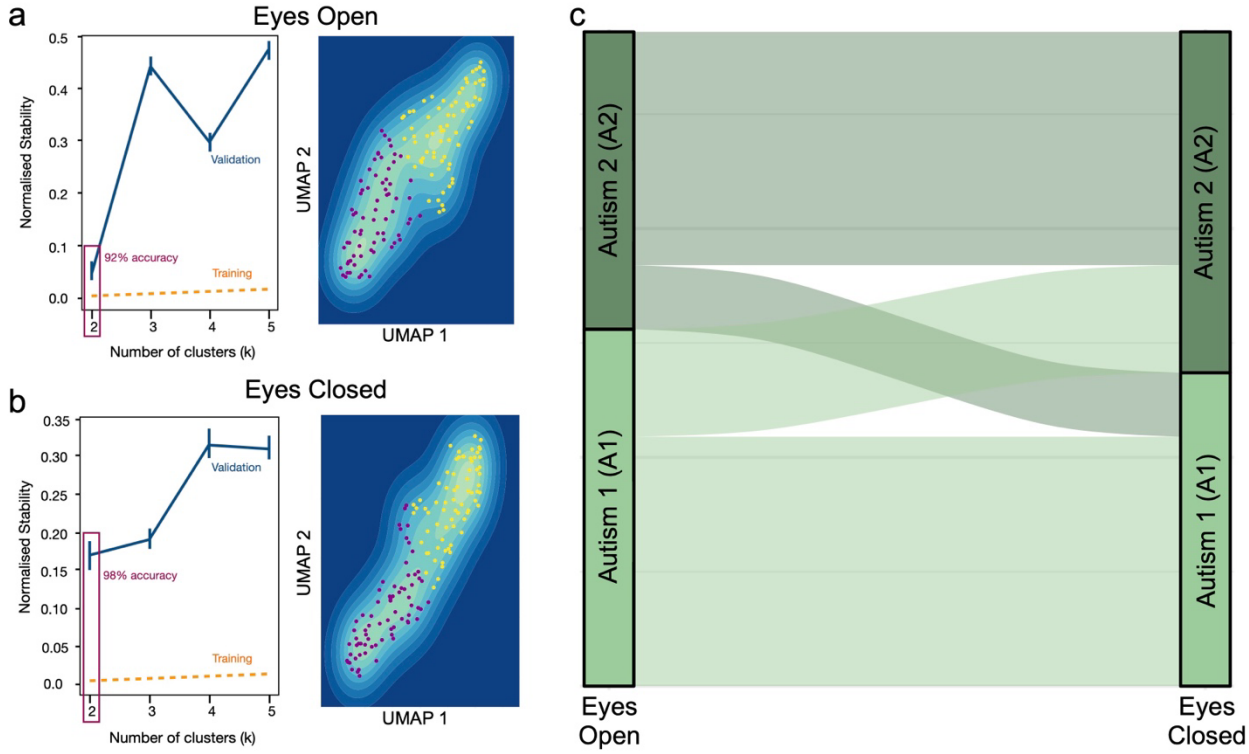

Figure 1: Identification of autism subtypes with high generalizability accuracy based EEG H data. *Panels A-B show normalized stability plots (eyes open, A; eyes closed, B) that indicate that a 2-cluster solution minimizes clustering stability and produces high generalizability accuracy (92-98%) in independent data. The UMAP plots next to the stability plots show evidence that the*

clusters highly deviate from the null single multivariate Gaussian distribution. Panel C shows an alluvial plot to indicate how consistent are the 2 subtypes across eyes open and eyes closed conditions.

Autism E:I neurosubtypes differ from typical development in opposite directions

We next proceeded to test for differences between autism E:I neurosubtypes relative to a typically-developing (TD) comparison group. Linear mixed effect models were used with H values at each electrode as the dependent variable. Subtype, age, and their interaction were fixed effects in the model, while acquisition site and repeat blocks were modeled as random effects (see Methods). We found a significant main effect of subtype across all electrodes. Specific between-group comparisons of TD vs autism subtype 1 and TD vs autism subtype 2 show that the group difference here is driven by both autism subtypes being significantly different from TD. Autism subtype 1 had higher H (i.e. lower E:I ratio) compared to TD (eyes open condition: *Cohen's d* > 0.27, *mean d* = 0.49; eyes closed condition: *Cohen's d* > 0.25, *mean d* = 0.51) (Figure 2A-B; Supplementary Table 3). While the group differences are relatively strong across all electrodes, the topographies of effect size for TD vs autism subtype 1 shown in Figure 2B indicate relatively larger differences over central and posterior electrodes. In contrast, autism subtype 2 showed the opposite effect of lower H (i.e. higher E:I ratio) compared to TD (eyes open condition: *Cohen's d* < -0.52; *mean d* = -0.71; eyes closed condition: *Cohen's d* < -0.62, *mean d* = -0.79) (Figure 2A-B). These effects were all remarkably consistent over repeated blocks, which further emphasizes the robustness of the effects (Figure 2C). While group differences are relatively strong across all electrodes, the topographies of effect size for TD vs autism subtype 2 shown in Figure 2B indicate relatively larger differences over temporo-parietal electrodes. Lower H in autism subtype 2 is indicative of a higher E:I ratio and is compatible with the predictions from the original E:I theory[1]. However, the existence of the opposing autism subtype 1, with higher H (i.e. lower E:I ratio), is compatible with a more updated view about E:I imbalance in autism which suggests that imbalance towards either extreme may be important[2,3]. The subtypes are not equally deviant compared to the TD group though, as autism subtype 2 tends to show a more extreme deviation than autism subtype 1. In sum, the evidence here showcases an important validation that idiopathic autistic males can be described by E:I imbalances that deviate from the TD population in either direction and underscores the point about atypical E:I imbalance being a concept that deviates from optimal E:I balance.

In addition to main effects of subtype, we also identified ubiquitous main effects of age involving a majority of all electrodes in the eyes open condition and primarily central and occipital electrodes in the eyes closed condition (Supplementary Figure 1A-B; Supplementary Table 3). These effects are described as a negative relationship between H and age (Supplementary Figure 1C-D) and are congruent with other literature on E:I-sensitive metrics (e.g., 1/f slope) and how they change in a similar direction as one ages[9–11]. Finally, given the lack of any significant subtype*age interactions, it is clear that these age effects do not manifest differentially as a function of subtype membership (Supplementary Table 3).

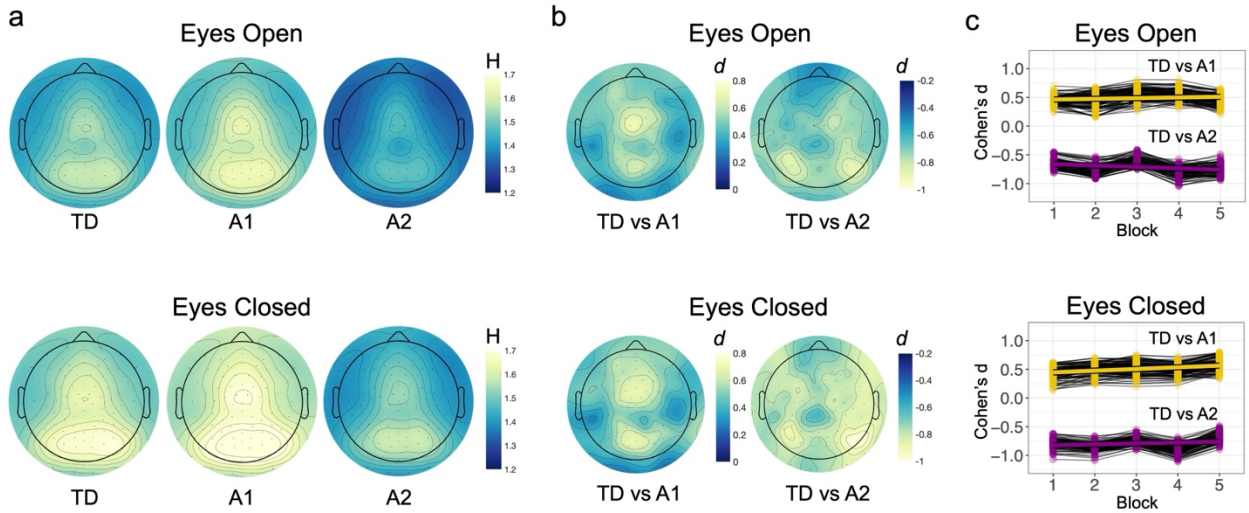

Figure 2: Differences between autism subtypes and TD across all electrodes. *Panel A (left) shows block-averaged H topographies for eyes open (top) and eyes closed (bottom) conditions. After statistical testing, we quantified the effect size difference between autism subtypes and TD. These effect size topographies are shown in panel B (middle), whereby we see that autism subtype 1 has ubiquitously increased H across all electrodes, whereas autism subtype 2 has ubiquitously decreased H across all electrodes. Panel C (right) shows the effect sizes plotted for all electrodes and across each of the 5 blocks. These plots show that the effect sizes remain relatively consistent over 5 repeat blocks of eyes open or closed conditions.*

Given that statistically significant main effects of subtype were present across the scalp, this potentially indicates that H variance manifests as a global factor. To better understand whether differential subtype H variance is best explained by this global or other local factors, we next proceeded to use principal components analysis (PCA) to decompose scalp-wide H variance into orthogonal components with different spatial topographies. PC1 explains a large majority of scalp-wide H variance (eyes open = 67.1%; eyes closed = 66.6%) and is spatially homogeneous across the scalp. This homogenous topography is indicative of PC1 being a global component. Three other PCs were also identified, and cumulatively with PC1, account for ~80% of the total variance in H (Supplementary Figure 2). These subsequent PCs show a much more specific and localized spatial topography. Thus, beyond the global H signal capture by the large PC1 component, there are smaller components explaining how H more subtly varies in a spatially-specific manner.

We next ran similar linear mixed effect models testing subtype, age, and subtype*age interactions on these first 4 PCs (Supplementary Table 4). This was done in order to test in a more principled manner whether the subtypes are differentiated by global and/or local components of H variation. Results for PC1 are similar across both eyes open and eyes closed conditions, with no subtype*age interactions (eyes open: $F = 2.42$, $p_{fdr} = 0.359$; eyes closed: $F = 0.80$, $p_{fdr} = 0.756$), but significant main effects of age (eyes open: $F = 16.32$, $p_{fdr} = 2.73\text{E-}04$; eyes closed: $F = 9.3$, $p_{fdr} = 0.005$) and subtype (eyes open: $F = 144.95$, $p_{fdr} = 3.38\text{E-}46$; eyes closed: $F = 180.38$, $p_{fdr} = 6.48\text{E-}56$). The main effect of age manifests as a negative relationship (i.e. decreasing PC1 scores with increasing age) (Supplementary Figure 1E-F). The main effect of subtype manifests with autism subtype 1 having higher values compared to TD (eyes open: $t = 7.06$, $p_{fdr} = 6.45\text{E-}11$, *Cohen's d* = 0.62; eyes closed: $t = 6.79$, $p_{fdr} = 2.91\text{E-}10$, *Cohen's d* = 0.65), but autism subtype 2 showing lower values compared to TD (eyes open: $t = -8.57$, $p_{fdr} = 3.06\text{E-}15$, *Cohen's d* = -0.93 ;

eyes closed: t = -9.83, p_{fdr} = 6.52E-19, *Cohen's d* = -1.04) (Figure 3A-B). Thus, results from PC1 captures the same types of effects observed in prior analyses per each electrode.

During the eyes open condition, PC4 was the only other component to show a significant main effect of subtype and with significant differences between TD and the autism neurosubtypes (F = 3.53, p = 0.03 p_{fdr} = 0.061; TD vs A1: t = 2.19, p_{fdr} = 0.04; TD vs A2: t = 2.46, p_{fdr} = 0.029; Supplementary Table 4). The topography of PC4 shows differentiation between frontal and temporal electrodes (Figure 3C). Given the combination of PC1 and PC4 subtype effects during the eyes open condition, we next reconstructed the data exclusively based on PC1 and PC4 in order to descriptively show how subtype main effects manifest. Here we see that H is elevated in autism subtype 1 compared to TD and this effect is most prominent over frontal and posterior electrodes compared to temporal electrodes (Figure 3D). In contrast, H is decreased in autism subtype 2 compared to TD, and this effect is strongest over non-frontal electrodes (Figure 3E).

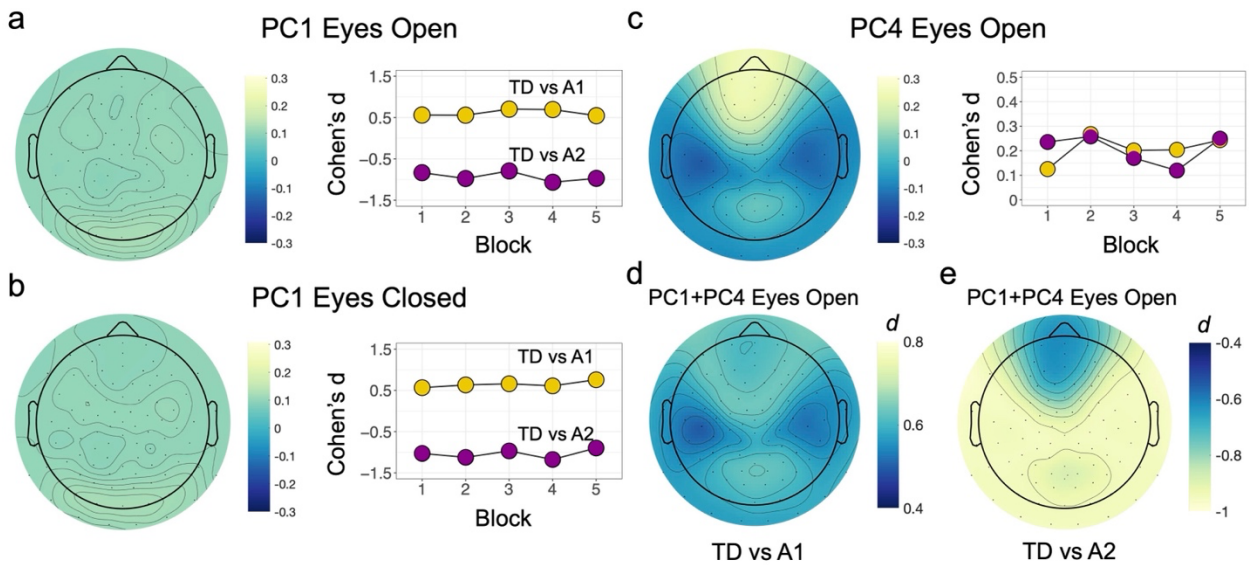

Figure 3: PCA decomposition of global versus local components of H that differ significantly between autism neurosubtypes and TD. *Panel A and B show PC1 for eyes open (top) and eyes closed (bottom) conditions. The topography of PC1 is shown on the left, with similar loadings across all electrodes, indicating that it is a global component explaining a large majority of the H variance. Effect size plots are shown to the right of the topography plots and indicate remarkable consistency of effect size across repeat blocks. Panel C shows the topography and effect sizes for the significant main effect of subtype in PC4 during the eyes open condition. PC4's topography has strong loading over frontal electrodes and opposing effects at over temporal electrodes. Reconstructing PC1 and PC4 back to original H space shows increased H in autism subtype 1 compared to TD that is most prominent over frontal and posterior electrodes relative to temporal electrodes (D). In contrast, H is decreased in autism subtype 2 relative to TD and this effect is most prominent over non-frontal electrodes (E).*

Differential brain-behavior relationships

We next sought to test for phenotypic differences between these neurally-defined H autism subtypes in age, FIQ, and autism symptomatology (e.g., ASSQ, SCQ, SRS, RBS). None of these

variables showed significant differences between subtypes that were consistent across eyes open and eyes closed conditions (see Supplementary Table 5 for full set of statistical comparisons for all dependent variables) (Supplementary Figure 3). Although on-average phenotypic differences were not strong between the subtypes, it is possible that relationships between H and these phenotypic measures may be different. To test this hypothesis, we used partial least squares (PLS) correlation analysis[12]. This analysis identified one significant latent variable pair for both the eyes open (d = 6.09, p = 3.99e-4, percentage covariance explained = 33.1%) and eyes closed (d = 9.79, p = 2.99e-4, percentage covariance explained = 64.61%) conditions. Effects in both eyes open and eyes closed conditions are likely driven by a global effect spread across the scalp, as PLS brain bootstrap (BSR) ratios are widely greater than 2 across all electrodes (Fig 4A-B). In terms of the behavioral variables that drive these brain-behavior relationships, we see some evidence suggesting that age, SCQ, and SRS are important (Fig 4C-D), primarily in TD and autism subtype 1. Across eyes open and eyes closed, these effects are highly preserved within both autism subtypes (autism subtype 1: r = 0.88, p = 0.001; autism subtype 2: r = 0.84, p = 0.004). However, the effects in the TD group are not as highly preserved across eyes open and eyes closed (r = 0.51, p = 0.15). This relatively weaker preservation across eye viewing conditions in TD may explain why age, SCQ, and SRS correlations change in the TD group across eyes open or closed conditions. The weaker preservation in TD may also be indicative of higher sensitivity to neural changes of behavioral relevance in TD across relatively simple eye viewing condition changes. In contrast to the variables of importance for TD and autism subtype 1, the only variable with a strong driving effect in autism subtype 2 is age and this effect is consistent across eyes open and eyes closed conditions (Fig 4C-D). The relationship here is negative and implies that with increasing age, H decreases (i.e. higher E:I ratio) in autism subtype 2.

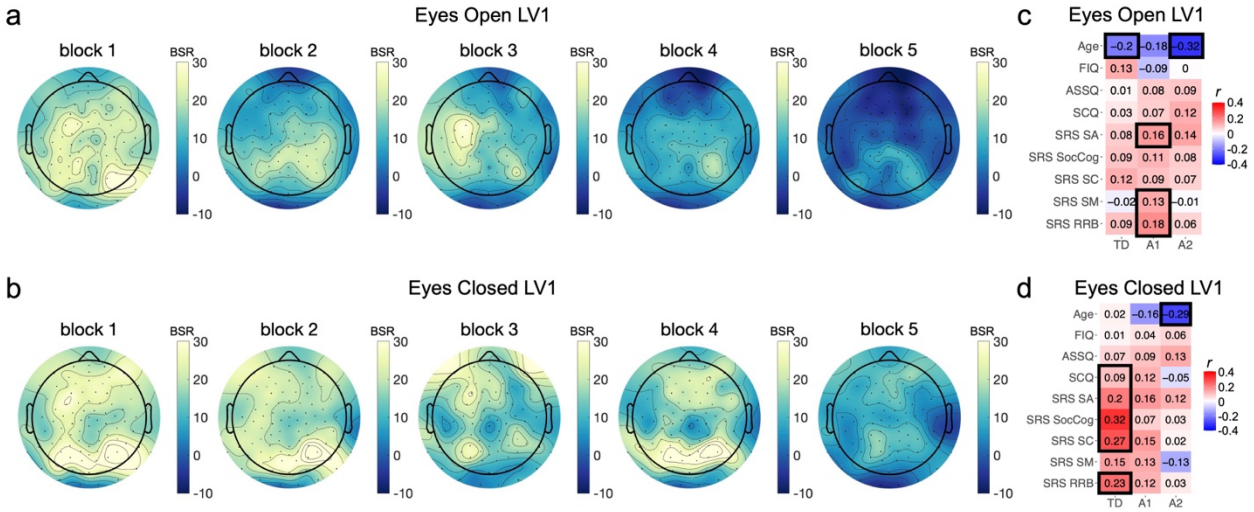

Figure 4: Subtype-specific brain-behavior relationships. *PLS analysis identified one latent variable pair, LV1, within eyes open and eyes closed conditions that shows a statistically significant multivariate brain (H) by behavioral relationship. Panels A and B show brain bootstrap ratios (BSR) from PLS LV1 across all electrodes and all blocks in the eyes open (A) and eyes closed (B) conditions. Brain BSRs > 2 are generally considered strong drivers of the PLS relationship, and here all electrodes have brain BSRs well over 2. Panels C and D show PLS behavior scores (i.e. correlations per each variable) to illustrate strength and stability of relationships driving the PLS latent variable pair LV1. These heatmaps show correlation values with H and cells with a black outline are those with 95% confidence intervals that do not include*

a value of zero, and thus, are strong and stable contributors to the LV1 relationships observed in eyes open (C) and eyes closed (D) conditions.

Discussion

In this work, we examined an EEG-based biomarker of E:I imbalance known as the Hurst exponent (H) in idiopathic autistic males. Our past work has shown that H computed from neural time-series data is related to underlying differences in E:I ratio[5]. Here we estimated H in EEG measured across the scalp and then used unsupervised data-driven clustering methods to test whether E:I-defined neurosubtypes can be identified and to what extent such neurosubtypes might be generalizable to the autism population. We find evidence supporting the idea that there are 2 robust and reproducible E:I neurosubtypes and that such subtypes can be identified with 92-98% accuracy in new independent data. Alongside our other past work taking a similar relative clustering validation approach[6,13,14], this work showcases that we can begin with unsupervised data-driven discoveries and then immediately translate those discoveries into supervised prediction and classification models. Further utilization of such robust, reproducible, and highly generalizable stratification models may be useful for future work in the field. The robustness of the observed subtypes can also be seen in the remarkable consistency of the subtype labels across eyes open versus eyes closed conditions in a large majority of individuals, and by the consistency of effect sizes across repeated blocks of eyes open and eyes closed conditions.

Regarding the description of the identified autism subtypes, we find that autism subtype 1 is characterized by globally lower E:I ratio (i.e. higher H) compared to TD controls, while autism subtype 2 is characterized by globally higher E:I (i.e. lower H) compared to TD, which is most prominent over non-frontal electrodes. The current sample was roughly split in half by these subtypes, indicating that one subtype does not necessarily adequately describe all autistic individuals. The most updated version of the E:I theory of autism predicts that E:I imbalance is affected in autism in either direction compared to what is considered an optimal level of balance defined by what is normative in the typically-developing brain[3]. Our findings provide empirical validation of this prediction by showing that around half of autistic males in our sample conform to either extreme. Thus, like other work examining heterogeneity in E:I mechanisms in autism[5], this work provides further evidence that dysregulation of E:I in autism can take many forms and may need to be personalized with respect to the type of individual in question.

Another observation from the current results is the remarkably global effect of H in these subtypes. While spatial specificity is a limitation behind EEG data, it is remarkable that most of the effects derived in this work are those that are global in nature across the entire scalp, rather than more localized in topography. The subtle exception to this was a small effect specific to the eyes open condition isolated in PC4. PC4 spatially varies in a manner that distinguishes frontal and temporal electrodes. Reconstructing the data based on PC1 and PC4 components shows that the global attenuation of H in autism subtype 2 is most pronounced over non-frontal electrodes. In contrast, the elevation of H in autism subtype 1 is most pronounced over frontal and posterior electrodes. Thus, the subtypes are different not only in the directionality of their difference relative to TD, but also in the topography of effects, potentially indicative of differential impact of separate brain regions. It is unclear how such results may hold up against other past work looking at H or related measures in autism in EEG[15,16] and rsfMRI data[5,17–19]. Such past work does not examine

data-driven E:I subtypes and instead rely on the clinical diagnosis to conduct case-control modeling. Future work applying such data-driven subtyping models will allow us to see how well these observations generalize across EEG and fMRI data and across autistic individuals at different points in the lifespan. Given the lack of more precise spatial sensitivity for localizing these observed atypical EEG E:I effects, future work examining these kinds of subtypes with rsfMRI may be important. It could be that E:I mechanisms may be differentially altered along spatial gradients of macroscale neural organization such as sensory-association cortex hierarchy[20], which are also known to be sensitive to differences in intrinsic neural time-scale gradients and E:I mechanisms[21,22].

Finally, we found little evidence of on-average subtype differences in demographic and behavioral measures such as age, IQ, and autism-specific symptomatology. This suggests that E:I neurosubtypes are not immediately self-evident via proxies of dramatically different phenotypic profiles alone. Rather, what is more sensitive to explaining behavioral phenotypic effects are the subtype labels combined with individual-level variation in H. PLS modeling allowed us to identify a significant multivariate brain-behavioral relationship that manifests differently between the 2 autism E:I neurosubtypes. Autistic traits, as measured by the SRS, are positively associated with increasing global H in autism subtype 1 during the eyes open condition. This effect is relatively preserved during the eyes closed condition and also evident in TD. Thus, the effect here may be indicative of a continuum for how E:I biology may be related to autistic traits in TD and autism subtype 1. In contrast, a similar type of relationship was not apparent between SRS and H in autism subtype 2. Given that continuous variation in autistic traits may be mediated by heritable polygenic risk mechanisms[23,24], these results may be suggestive that the differential E:I neurophenotype in autism subtype 1 may be mediated by different neurobiological and genomic mechanisms compared to autism subtype 2. Thus, a potential inference from these results is that E:I autism neurosubtypes may be more enriched for different types of genomic and neurobiological mechanisms. Identification of E:I neurosubtypes with differential brain-behavioral relationships may also be important for translational research to facilitate more positive outcomes for specific types of individuals. Given prerequisite pre-treatment EEG datasets, current or future clinical trials focusing on pharmacological agents that manipulate/alter E:I-relevant mechanisms could be designed and/or re-analyzed in ways that take into account such stratification biomarkers[25]. Such an approach might yield more powerful and personalized insight into how such E:I-relevant agents may exert an effect (if any) on important clinical outcomes.

There are some limitations and caveats to underscore about the current work. First, the data only examine males. Examination of females was not included due to limited sample size. However, given the potential that E:I mechanisms may not operate the same way in autistic males versus females[5], future work examining females is needed. Second, although the IQ distributions in autism extend into the lower ranges, a majority of autistic individuals falls within 2 standard deviations of the TD norm. Thus, generalizing this work to autistic individuals with very low IQ may be limited. Third, the minimum age in our sample was 5 years and thus, our ability to generalize to even younger individuals may be limited. Given that E:I mechanisms tend to change with age (Supplementary Figure 1)[9–11], more work is needed examining these types of metrics at the earliest ages autism can be diagnosed. The current version of the E:I theory[2,3] allows for the possibility that E:I imbalance may arise because of core pathophysiology versus compensatory effects. As individuals age, there may be higher likelihood that E:I phenotypes may be indicative

of compensatory effects. Fourth, future work should examine these subtypes and biomarkers in individuals that are better characterized in terms of genomic mechanisms. This will better elucidate the impact of differential genomic mechanisms (e.g., high impact rare variants versus polygenic risk) on the subtypes. Finally, our work here is restricted to what occurs during resting state eyes open and eyes closed conditions. It is possible that when processing dynamic naturalistic stimuli and/or across specific cognitive tasks or conditions[26,27] different results might arise. Thus, future work examining E:I-relevant biomarkers and stratifications is needed across a range of conditions, stimuli, and contexts (e.g., social interaction) that might better capture the types of situations autistic individuals exhibit strengths and/or weaknesses.

In conclusion, we have discovered that idiopathic autistic males can be split into E:I neurosubtypes based on EEG data collected during resting state conditions. These neurosubtypes exhibit opposing effects in relation to a TD comparison group and are differentially related to phenotypic measures. Future work expanding on these insights may extend the work into females, individuals with more extreme IQ profiles, younger ages, and more comprehensive genomic characterization. Finally, the work could provide a basis for examining how E:I mechanisms may be affected in other cognitive states and/or while processing other types of stimuli.

Methods

CMI-HBN dataset

To identify autism E:I neurosubtypes, we utilized EEG and phenotypic data from data releases 1-10 of the Child Mind Institute Healthy Brain Network (CMI-HBN) dataset. The CMI-HBN is an initiative to create a biobank of individuals aged 5-21 from the New York area. Participants undergo diagnostic and phenotypic assessments, EEG and MRI scanning during resting state, naturalistic viewing and task conditions. Data was acquired at four sites in the New York area - Staten Island, Midtown, Harlem, and a mobile unit. The CMI-HBN initiative received ethical approval by the Chesapeake Institutional Review Board, and written informed consent was obtained from all participants or their legal guardians (for participants < 18 years). For further details on the CMI-HBN initiative see Alexander et al., 2017[8].

For this work we started by isolating all participants from data releases 1-10 that had a diagnosis of autism (n = 412) or who were typically-developing (TD), as indicated by the label 'No Diagnosis Given' (n = 257). From this pool of data, we excluded participants with missing resting state EEG data (n = 15) or whose data could not be successfully preprocessed (n = 106). Given a low sample size of female participants with autism (n = 50) and a potential sex-bias on the Hurst exponent, female participants (n = 139) were also excluded. The final sample size was of n = 286 autistic males and n = 123 typically developing males. The Wechsler Adult Intelligence Scale (WAIS), Wechsler Abbreviated Scale of Intelligence (WASI) and Wechsler Intelligence Scale for Children (WISC) were selected as measures of full-scale IQ (FIQ), while the Social Responsiveness Scale (SRS-2), Repetitive Behavior Scale (RBS-R), Social Communication Questionnaire (SCQ) and Autism Spectrum Screening Questionnaire (ASSQ) were selected as clinical phenotypic measures. See Table 1 for a summary of participant characteristics.

EEG data acquisition

EEG data was recorded using a 128-channel EEG geodesic hydrocel system (Electrical Geodesics Inc; EGI). Data was recorded at a sampling rate of 500 Hz, with a bandpass filter of 0.1 to 100 Hz and reference at the vertex of the head (Cz). Resting state data was collected for 5 minutes, while the participant sits in front of a screen with a fixation cross on the center. Throughout the recording, participants alternate having their eyes open (20 seconds blocks) and closed (30 seconds blocks) for five blocks.

EEG data preprocessing

In order to handle in a reproducible way large amount of data, we developed a semi-automated preprocessing pipeline that combines a set of custom MATLAB scripts executable within the EEGLAB[28] framework with other associated software (ASR[29,30] and IClabel[31]). The pipeline consists of a sequence of steps. Step one consists of removal of the outer ring of channels (26 channels) that are mainly located on the face and the neck and generally with a defective contact with the skin surface. Data is then downsampled to 250Hz (one sample every 4ms) and a basic FIR filter (*filtfilt.m* function) with a high pass cutoff of 1Hz and a low pass cutoff of 80 Hz is applied. Line noise is removed via a notch filter centered at 60 Hz +/-2. Bad channels are identified based on a combination of three different parameters: 1) flatline duration (for more than 5 consecutive seconds); 2) standard deviations (> 4) as compared to the total channel signal; 3) correlation with the neighboring channels (lower than the default value of 0.8). Channels falling into one of these conditions are rejected and interpolated with a spherical method. In a further step the Artifact Subspace Reconstruction (ASR) algorithm is applied to detect data segments contaminated by non-stereotypical artifacts. A preliminary calibration of the rejection threshold criteria is computed on a 'cleaner' portion of the EEG signal. Then ASR identifies the artifact subspace and repairs the artifactual samples based on the predefined threshold values. After re-referencing to the average of all sensors, the number of channels is further reduced by 10% to match the number of available samples inputted into independent component analysis (ICA with icatype set to 'runica'). The resulting components are classified by the ICLabel algorithm as deriving from 'brain' or a variety of non-brain sources (e.g., muscle, line noise, channel noise, eye, or other). The non-brain ICs (probability < 20% of being 'brain') are then projected out from the data. After preprocessing was complete, we output preprocessing reports that could be manually checked and classified for exclusion or inclusion into further downstream data analysis. For this data quality control step, all preprocessing reports were manually inspected by MVL and a subset of overlapping subjects were also inspected by NB and AV. From this data quality control check we excluded participants for a variety of qualitative and quantitative reasons, including issues with the raw time-series data, large numbers of bad channels or bad samples that could not be repaired, too few high probability brain independent components (IC) in the top-35 ranked ICs, and/or odd looking IC topographies amongst ICs labeled as 'brain'. For examples of excluded and included participants, see Supplementary Figure 4. Data quality metrics such as number of bad channels and percentage of bad samples were computed for all participants retained for further downstream analysis and were used for further denoising steps before the subtyping analysis.

EEG subtyping analysis

For EEG-based neural features relevant to E:I imbalance, we computed the Hurst exponent (H). Prior work has validated the use of H to infer E:I mechanisms from neural time-series data[5], whereby lower H values are indicative of increased E:I ratio. H was computed at each electrode for each of the five blocks of eyes open or eyes closed conditions with the *bfn_mfin_ml.m* function from the *nonfractal* MATLAB library (https://github.com/wonsang/nonfractal). After computing H for each participant and electrode, we implemented a denoising procedure to remove variance associated with data quality metrics from the preprocessing such as number of bad channels and percentage of bad samples. This denoising step was implemented via a linear model with H as the dependent variable and diagnosis, age, study site, number of bad channels, and percentage of bad samples as independent variables. Beta coefficients for number of bad channels and percentage of bad samples were isolated and then projected out of the data to adjust H values for these metrics. This procedure was done to ensure that any residual effects of data quality were handled before subtyping analysis was implemented. Denoised H data was then utilized in all further downstream analyses.

The primary subtyping analysis was implemented with stability-based relative clustering validation, otherwise known as *reval*[6]. With *reval* we aim to identify unsupervised data-driven clusters based on H within the autism sample (n = 286) and to identify the optimal number of clusters with cross-validation and test generalizability in new independent data. A 50-50 split was used to separate data into the initial training and validation sets. These sets were balanced for presence or absence of comorbid ADHD diagnosis and age and then preprocessed by scaling it to a mean of 0 and a standard deviation of 1. We also applied a preprocessing step of reducing the dimensionality of the data to 2 dimensions with Uniform Manifold Approximation and Projection (UMAP)[32] (number of neighbors = 30, number of components = 2, minimum distance = 0, random state seed = 24). The UMAP transformations derived from the training set were then applied to the validation set. After preprocessing we implement the primary steps within the reval pipeline - clustering and then producing a classifier that can predict clustering labels on held-out data. The clustering algorithm used throughout is k-means clustering, and the classifier was a k-nearest neighbor classifier (k=3). *reval* utilizes the training data within an internal 2-fold cross-validation loop to identify the optimal k clusters that minimizes clustering stability. This process is repeated 100 times to identify the best cluster solution. Once the optimal k is identified in the internal cross-validation of the training data, a classifier is fit to predict those cluster labels in new data. K-means clustering with the identified optimal k is then applied to the held-out validation set and then the classifier fit to the training data applied to the validation set with the goal of accurately predicting the clustering labels identified in the validation set. Generalization accuracy is then computed by comparing the actual clustering labels of validation set to the classifier's predicted labels. The generalization accuracy computed from *reval* on the validation set informs us as to how robust, stable, and reproducible are clustering labels in the autism population based on EEG H data. However, *reval* itself does not test the hypothesis of whether the clusters come from an underlying distribution a single or multiple Gaussians. The null hypothesis if clusters do not actually exist is that the clustering labels come from a single multivariate Gaussian distribution. Thus, to formally test the data with respect to this null hypothesis, we use the *sigclust* function within the *SigClust* R library to test whether the data deviates from this single multivariate Gaussian null distribution[33]. Finally, given that *reval* clustering is computed twice within the same individuals - once under eyes open and then again for eyes closed condition - this allowed the opportunity to examine consistency of subtype solutions across these two eye conditions. This was achieved descriptively by computing alluvial plots that allow us to visualize the percentage of individuals that stay within

the relatively same clustering subtype or which move to a different subtype across the eye conditions. For the individuals who changed subtypes across eyes open and eyes closed, we used linear modeling to test whether these types of individuals differed phenotypically (e.g., on age, FIQ, and autism symptomatology measures) from individuals who stayed within the same subtype.

Once autism EEG H subtypes were identified, we next tested for between-group differences between the autism subtypes and a typically-developing (TD) control group. For these analyses we utilized linear mixed effect models, computed per each electrode with the *lmer* function in the *lme4* R library. The dependent variable in these models were H values. Fixed effects of subtype, age and the subtype*age interaction were modeled as fixed effects of interest. Random effects in the model were acquisition site (random intercepts) and repeated measures such as block (random intercepts and slopes per each subject). Multiple comparison correction was implemented with false discovery rate (FDR; $q < 0.05$). Because electrode-wise analyses like these may be heavily redundant due to correlations between electrodes, we also utilized principal component analysis (PCA) as a more parsimonious way of summarizing H variation into global versus more localized E:I effects. Examination of scree plots from the PCA analysis showed an elbow after the first 5 PCs (Supplementary Figure 2), which explained ~85% of the variance in H. Thus, the first 5 PCs were retained for hypothesis testing under the same linear mixed effect model framework as described above. All fixed and random effects were the same as the previously described analysis. The main change is that PCs scores from each of the first 5 PCs are used as the dependent variable in the model. All between-group differences are descriptively shown in figures as standardized effect sizes, operationalized as Cohen's d in standard deviation units.

Behavioral and brain-behavior relationship analyses

Subtypes were tested for behavioral differences on age, FIQ, and autism symptomatology measures (e.g., ASSQ, SCQ, SRS, RBS) using linear models with the behavioral variable as the dependent variable and with subtype as the independent variable. Multiple comparison correction was achieved at FDR $q<0.05$. To test for brain-behavioral relationships we used a multivariate association analysis technique known as partial least squares (PLS) correlation analysis[12], which has been utilized extensively in our past work on autism subtyping[34–36]. For these analyses, we utilized behavioral variables of age, FIQ, ASSQ, SCQ and SRS subscales. The RBS was not utilized in the PLS analysis due to too much missing data. Two PLS analyses were computed - one per eyes open and eyes closed conditions. Groups (TD, autism 1, and autism 2) were input as blocked structures in the PLS analysis. Behavior-PLS analysis was utilized here, whereby H values are the multivariate brain matrix (i.e. the H matrix) and age, FIQ, and autism symptomatology measures are used as the multivariate behavioral matrix. For these analyses, repeat eyes open or eyes closed blocks were concatenated in the H matrix such that each individual or row in the matrix had 93 electrodes * 5 blocks (i.e. 465 H values). Statistical inference on latent variable pairs was achieved in the PLS analysis using permutation analysis (10,000 permutations). Brain bootstrap ratios (BSR) and 95% confidence intervals on behavior scores were computed via bootstrap resampling (10,000 resamples). Latent variable pairs were judged to be statistically significant based on permutation p-values being corrected with FDR $q<0.05$. Behavioral variables with 95% confidence intervals that do not include 0 are considered important for driving the relationship within the identified LV and are thus annotated in the figures describing the PLS results. Brain BSRs are typically considered important when BSRs exceed 2[12].

Data availability

CMI-HBN data can be found at http://fcon_1000.projects.nitrc.org/indi/cmi_healthy_brain_network/.

Code availability

The *reval* Python library can be found on GitHub (https://github.com/IIT-LAND/reval_clustering) and the documentation can be found at: https://reval.readthedocs.io. All analysis code for the study is available on our GitHub repo https://github.com/IIT-LAND/CMI_EEG_H.

Acknowledgments

This project was supported by funding from the Simons Foundation for Autism Research Initiative (SFARI; grant number 982347) to MVL and from the European Research Council (ERC) under the European Union's Horizon 2020 research and innovation programme (grant agreement No 755816; AUTISMS) to MVL.

Author Contributions

Conceptualization: MVL. Methodology: MVL, NB, AV, VM. Formal analysis: MVL, NB, AV, VM. Investigation: MVL, NB. Writing - original draft preparation: MVL, NB, DB, AV, VM. Writing - review and editing: MVL, NB, AV, DB, VM. Visualization: MVL, NB. Supervision: MVL. Project administration: MVL. Funding acquisition: MVL.

Competing Interests

The authors declare no competing interests.

References

1. Rubenstein, J.L.R., and Merzenich, M.M. (2003). Model of autism: increased ratio of excitation/inhibition in key neural systems. Genes Brain Behav. *2*, 255–267. 10.1034/j.1601-183x.2003.00037.x.

2. Nelson, S.B., and Valakh, V. (2015). Excitatory/Inhibitory Balance and Circuit Homeostasis in Autism Spectrum Disorders. Neuron *87*, 684–698. 10.1016/j.neuron.2015.07.033.

3. Sohal, V.S., and Rubenstein, J.L.R. (2019). Excitation-inhibition balance as a framework for investigating mechanisms in neuropsychiatric disorders. Mol. Psychiatry *24*, 1248–1257. 10.1038/s41380-019-0426-0.

4. Willsey, H.R., Willsey, A.J., Wang, B., and State, M.W. (2022). Genomics, convergent neuroscience and progress in understanding autism spectrum disorder. Nat. Rev. Neurosci. *23*, 323–341. 10.1038/s41583-022-00576-7.

5. Trakoshis, S., Martínez-Cañada, P., Rocchi, F., Canella, C., You, W., Chakrabarti, B., Ruigrok, A.N., Bullmore, E.T., Suckling, J., Markicevic, M., et al. (2020). Intrinsic excitation-inhibition imbalance affects medial prefrontal cortex differently in autistic men versus women. eLife *9*, e55684. 10.7554/eLife.55684.

6. Landi, I., Mandelli, V., and Lombardo, M.V. (2021). reval: A Python package to determine best clustering solutions with stability-based relative clustering validation. Patterns N. Y. N *2*, 100228. 10.1016/j.patter.2021.100228.

7. Hong, S.-J., Vogelstein, J.T., Gozzi, A., Bernhardt, B.C., Yeo, B.T.T., Milham, M.P., and Di Martino, A. (2020). Toward Neurosubtypes in Autism. Biol. Psychiatry *88*, 111–128. 10.1016/j.biopsych.2020.03.022.

8. Alexander, L.M., Escalera, J., Ai, L., Andreotti, C., Febre, K., Mangone, A., Vega-Potler, N., Langer, N., Alexander, A., Kovacs, M., et al. (2017). An open resource for transdiagnostic research in pediatric mental health and learning disorders. Sci. Data *4*, 170181. 10.1038/sdata.2017.181.

9. Voytek, B., Kramer, M.A., Case, J., Lepage, K.Q., Tempesta, Z.R., Knight, R.T., and Gazzaley, A. (2015). Age-Related Changes in 1/f Neural Electrophysiological Noise. J. Neurosci. Off. J. Soc. Neurosci. *35*, 13257–13265. 10.1523/JNEUROSCI.2332-14.2015.

10. Donoghue, T., Haller, M., Peterson, E.J., Varma, P., Sebastian, P., Gao, R., Noto, T., Lara, A.H., Wallis, J.D., Knight, R.T., et al. (2020). Parameterizing neural power spectra into periodic and aperiodic components. Nat. Neurosci. *23*, 1655–1665. 10.1038/s41593-020-00744-x.

11. Schaworonkow, N., and Voytek, B. (2021). Longitudinal changes in aperiodic and periodic activity in electrophysiological recordings in the first seven months of life. Dev. Cogn. Neurosci. *47*, 100895. 10.1016/j.dcn.2020.100895.

12. Krishnan, A., Williams, L.J., McIntosh, A.R., and Abdi, H. (2011). Partial Least Squares (PLS) methods for neuroimaging: a tutorial and review. NeuroImage *56*, 455–475. 10.1016/j.neuroimage.2010.07.034.

13. Mandelli, V., Landi, I., Busuoli, E.M., Courchesne, E., Pierce, K., and Lombardo, M.V. (2023). Prognostic early snapshot stratification of autism based on adaptive functioning. Nat. Ment. Health *1*, 327–336. 10.1038/s44220-023-00056-6.

14. Mandelli, V., Landi, I., Ceccarelli, S.B., Molteni, M., Nobile, M., D'Ausilio, A., Fadiga, L., Crippa, A., and Lombardo, M.V. (2023). Enhanced motor noise in an autism subtype with poor motor skills (Psychiatry and Clinical Psychology) 10.1101/2023.03.25.23287738.

15. Peck, F.C., Gabard-Durnam, L.J., Wilkinson, C.L., Bosl, W., Tager-Flusberg, H., and Nelson, C.A. (2021). Prediction of autism spectrum disorder diagnosis using nonlinear measures of language-related EEG at 6 and 12 months. J. Neurodev. Disord. *13*, 57. 10.1186/s11689-021-09405-x.

16. Catarino, A., Churches, O., Baron-Cohen, S., Andrade, A., and Ring, H. (2011). Atypical EEG complexity in autism spectrum conditions: a multiscale entropy analysis. Clin. Neurophysiol. Off. J. Int. Fed. Clin. Neurophysiol. *122*, 2375–2383. 10.1016/j.clinph.2011.05.004.

17. Lai, M.-C., Lombardo, M.V., Chakrabarti, B., Sadek, S.A., Pasco, G., Wheelwright, S.J., Bullmore, E.T., Baron-Cohen, S., MRC AIMS Consortium, and Suckling, J. (2010). A shift to randomness of brain oscillations in people with autism. Biol. Psychiatry *68*, 1092–1099. 10.1016/j.biopsych.2010.06.027.

18. Uscătescu, L.C., Hyatt, C.J., Dunn, J., Kronbichler, M., Calhoun, V., Corbera, S., Pelphrey, K., Pittman, B., Pearlson, G., and Assaf, M. (2022). Using the Excitation/Inhibition Ratio to Optimize the Classification of Autism and Schizophrenia (Psychiatry and Clinical Psychology) 10.1101/2022.05.24.22275531.

19. Watanabe, T., Rees, G., and Masuda, N. (2019). Atypical intrinsic neural timescale in autism. eLife *8*, e42256. 10.7554/eLife.42256.

20. Sydnor, V.J., Larsen, B., Bassett, D.S., Alexander-Bloch, A., Fair, D.A., Liston, C., Mackey, A.P., Milham, M.P., Pines, A., Roalf, D.R., et al. (2021). Neurodevelopment of the association cortices: Patterns, mechanisms, and implications for psychopathology. Neuron *109*, 2820–2846. 10.1016/j.neuron.2021.06.016.

21. Gao, R., van den Brink, R.L., Pfeffer, T., and Voytek, B. (2020). Neuronal timescales are functionally dynamic and shaped by cortical microarchitecture. eLife *9*, e61277. 10.7554/eLife.61277.

22. Wang, X.-J. (2020). Macroscopic gradients of synaptic excitation and inhibition in the neocortex. Nat. Rev. Neurosci. *21*, 169–178. 10.1038/s41583-020-0262-x.

23. Constantino, J.N., and Todd, R.D. (2003). Autistic traits in the general population: a twin study. Arch. Gen. Psychiatry *60*, 524–530. 10.1001/archpsyc.60.5.524.

24. Antaki, D., Guevara, J., Maihofer, A.X., Klein, M., Gujral, M., Grove, J., Carey, C.E., Hong, O., Arranz, M.J., Hervas, A., et al. (2022). A phenotypic spectrum of autism is attributable to the combined effects of rare variants, polygenic risk and sex. Nat. Genet. *54*, 1284–1292. 10.1038/s41588-022-01064-5.

25. Ahmad, J., Ellis, C., Leech, R., Voytek, B., Garces, P., Jones, E., Buitelaar, J., Loth, E., Dos Santos, F.P., Amil, A.F., et al. (2022). From mechanisms to markers: novel noninvasive EEG proxy markers of the neural excitation and inhibition system in humans. Transl. Psychiatry *12*, 467. 10.1038/s41398-022-02218-z.

26. Robertson, C.E., Ratai, E.-M., and Kanwisher, N. (2016). Reduced GABAergic Action in the Autistic Brain. Curr. Biol. CB *26*, 80–85. 10.1016/j.cub.2015.11.019.

27. Spiegel, A., Mentch, J., Haskins, A.J., and Robertson, C.E. (2019). Slower Binocular Rivalry in the Autistic Brain. Curr. Biol. CB *29*, 2948-2953.e3. 10.1016/j.cub.2019.07.026.

28. Delorme, A., and Makeig, S. (2004). EEGLAB: an open source toolbox for analysis of single-trial EEG dynamics including independent component analysis. J. Neurosci. Methods *134*, 9–21. 10.1016/j.jneumeth.2003.10.009.

29. Kothe, C.A.E., and Jung, T.-P. (2016). Artifact removal techniques with signal reconstruction.

30. Chang, C.-Y., Hsu, S.-H., Pion-Tonachini, L., and Jung, T.-P. (2020). Evaluation of Artifact Subspace Reconstruction for Automatic Artifact Components Removal in Multi-Channel EEG Recordings. IEEE Trans. Biomed. Eng. *67*, 1114–1121. 10.1109/TBME.2019.2930186.

31. Pion-Tonachini, L., Kreutz-Delgado, K., and Makeig, S. (2019). ICLabel: An automated electroencephalographic independent component classifier, dataset, and website. NeuroImage *198*, 181–197. 10.1016/j.neuroimage.2019.05.026.

32. McInnes, L., Healy, J., and Melville, J. (2020). UMAP: Uniform Manifold Approximation and Projection for Dimension Reduction. Preprint at arXiv.

33. Liu, Y., Hayes, D.N., Nobel, A., and Marron, J.S. (2008). Statistical Significance of Clustering for High-Dimension, Low–Sample Size Data. J. Am. Stat. Assoc. *103*, 1281–1293. 10.1198/016214508000000454.

34. Lombardo, M.V., Pierce, K., Eyler, L.T., Carter Barnes, C., Ahrens-Barbeau, C., Solso, S., Campbell, K., and Courchesne, E. (2015). Different functional neural substrates for good and poor language outcome in autism. Neuron *86*, 567–577. 10.1016/j.neuron.2015.03.023.

35. Lombardo, M.V., Pramparo, T., Gazestani, V., Warrier, V., Bethlehem, R.A.I., Carter Barnes, C., Lopez, L., Lewis, N.E., Eyler, L., Pierce, K., et al. (2018). Large-scale associations between the leukocyte transcriptome and BOLD responses to speech differ in

autism early language outcome subtypes. Nat. Neurosci. *21*, 1680–1688. 10.1038/s41593-018-0281-3.

36. Lombardo, M.V., Eyler, L., Pramparo, T., Gazestani, V.H., Hagler, D.J., Chen, C.-H., Dale, A.M., Seidlitz, J., Bethlehem, R.A.I., Bertelsen, N., et al. (2021). Atypical genomic cortical patterning in autism with poor early language outcome. Sci. Adv. *7*, eabh1663. 10.1126/sciadv.abh1663.

Tables

	Eyes Open		Eyes Closed		
	Autism Subtype 1	Autism Subtype 2	Autism Subtype 1	Autism Subtype 2	TD
Sample size (n)	141	145	142	144	123
Age in years (mean ± sd)	10.13 ± 3.28	11.45 ± 3.78	11.05 ± 3.45	10.55 ± 3.73	9.55 ± 3.27
FIQ (mean ± sd)	95.94 ± 18.26	94.6 ± 19.64	94.30 ± 20.3	96.23 ± 17.5	105.77 ± 15.35
ASSQ total (mean ± sd)	17.34 ± 10.11	19.38 ± 11.69	17.96 ± 10.73	18.78 ± 11.21	2.21 ± 3.15
RBS-R total (mean ± sd)	55.51 ± 39.82	54.51 ± 35.83	54.3 ± 39.46	55.66 ± 36.27	11.92 ± 18.05
SCQ total (mean ± sd)	11.91 ± 5.39	12.72 ± 5.96	12.21 ± 5.62	12.42 ± 5.77	5.48 ± 3.19
SRS-2 total (mean ± sd)	68.93 ± 10.54	70.57 ± 11.55	69.57 ± 11.16	69.96 ± 11.04	48.8 ± 6.89

***Table 1*: Sample size and descriptive statistics for age, intelligence and autism symptomatology for the autism E:I neurosubtypes and typically-developing (TD) comparison group.** *This table shows sample size (n) or mean and standard deviation (in parentheses) for autism E:I neurosubtypes and TD groups. Abbreviations: FIQ: full-scale intelligence quotient, ASSQ: Autism Spectrum Screening Questionnaire; RBS-R: Repetitive Behaviors Scale - Revised (RBS-R); SCQ: Social Communication Questionnaire; SRS-2: Social Responsiveness Scale 2.*

Supplementary Figures

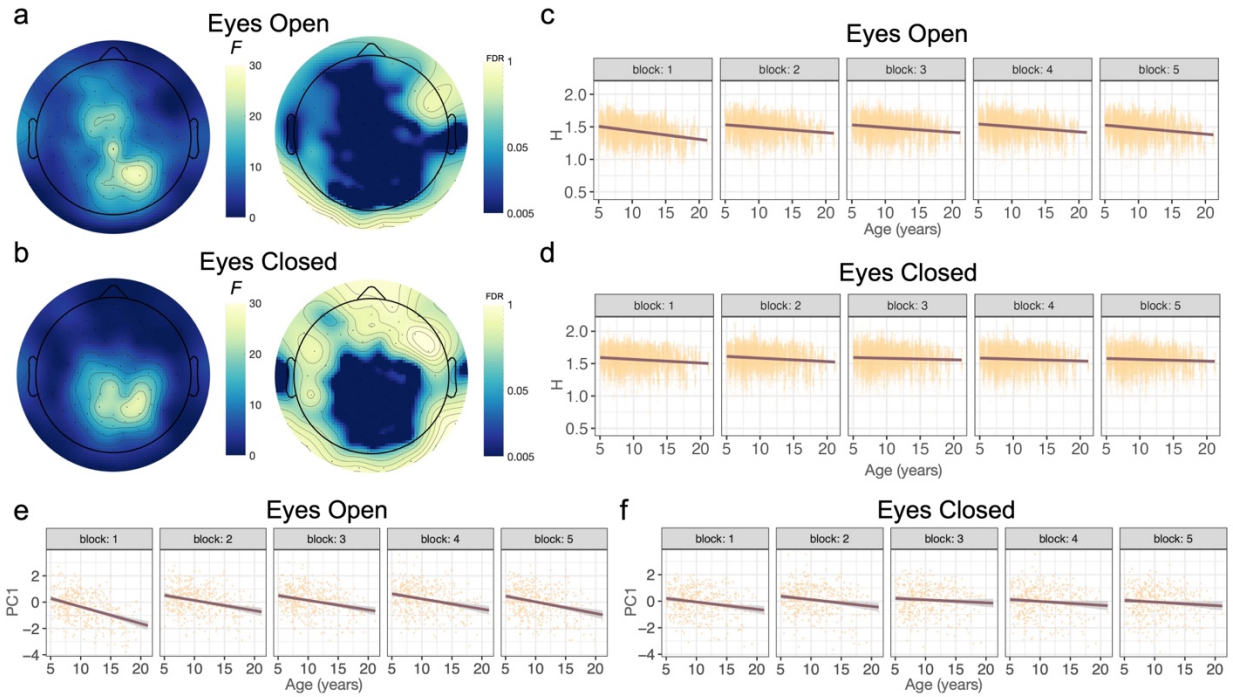

Supplementary Figure 1: Decreasing H with increasing age. *Panels A and B show topoplots of F-statistics of the main effect of age (left) along with FDR topoplots (right) to indicate which electrodes show such significant effects. Panels C and D show scatterplots of H (y-axis) over age (x-axis) for each block in eyes open (C) and eyes closed (D) conditions. Panels E and F show scatterplots of age (x-axis) by PC1 scores (y-axis) for eyes open (E) and eyes closed (F) conditions.*

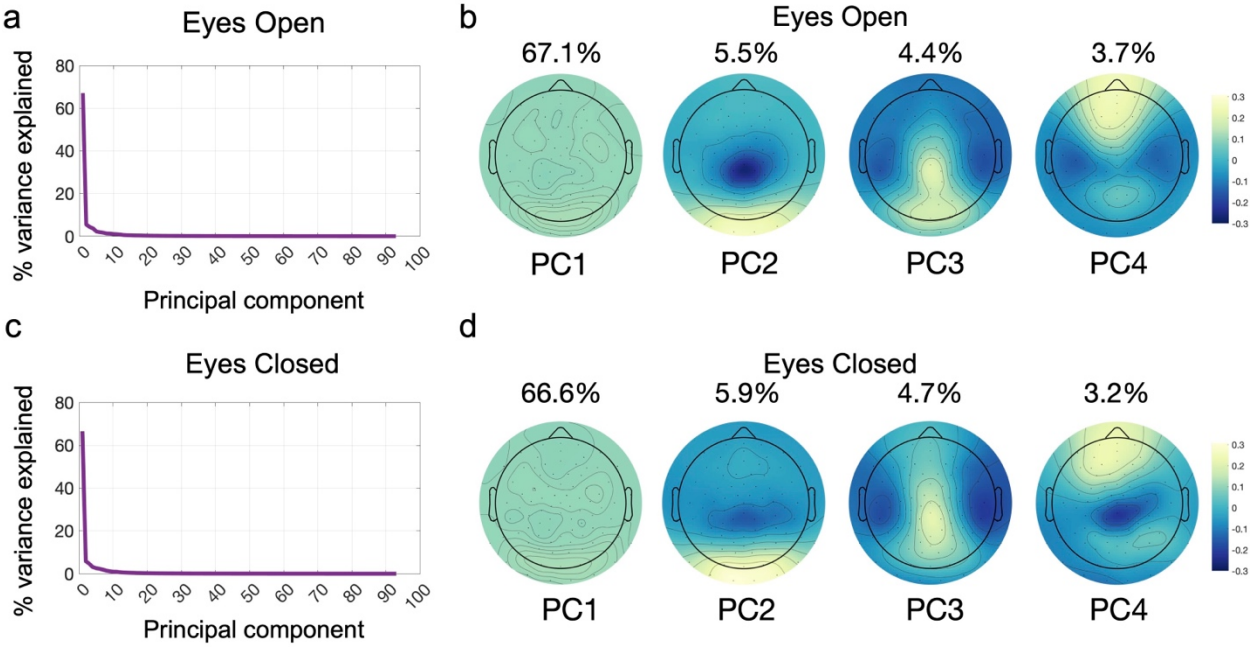

Supplementary Figure 2: PCA analysis isolates top 4 PCs explaining ~80% of the variance in scalp-wide H. *Panels A and C show scree plots of percentage variance explained (y-axis) for each PC (x-axis) for eyes open (A) and eyes closed (C) conditions. Panels B and D show topoplots of the loadings for eyes open (B) and eyes closed (C) conditions.*

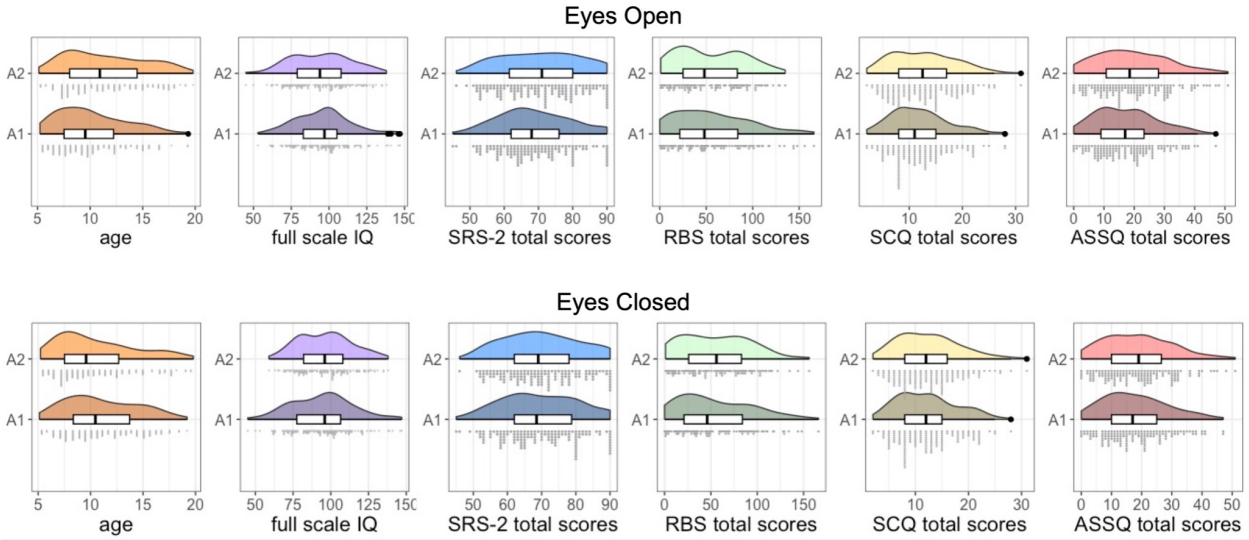

Supplementary Figure 3: Raincloud plots of behavioral variables for each autism E:I neurosubtype. *This plot shows the distribution of values over age, FIQ, and autism symptomatology measures (SRS, RBS, SCQ, and ASSQ) for eyes open (top) and eyes closed (bottom) conditions for both autism subtypes 1 (A1) and 2 (A2).*

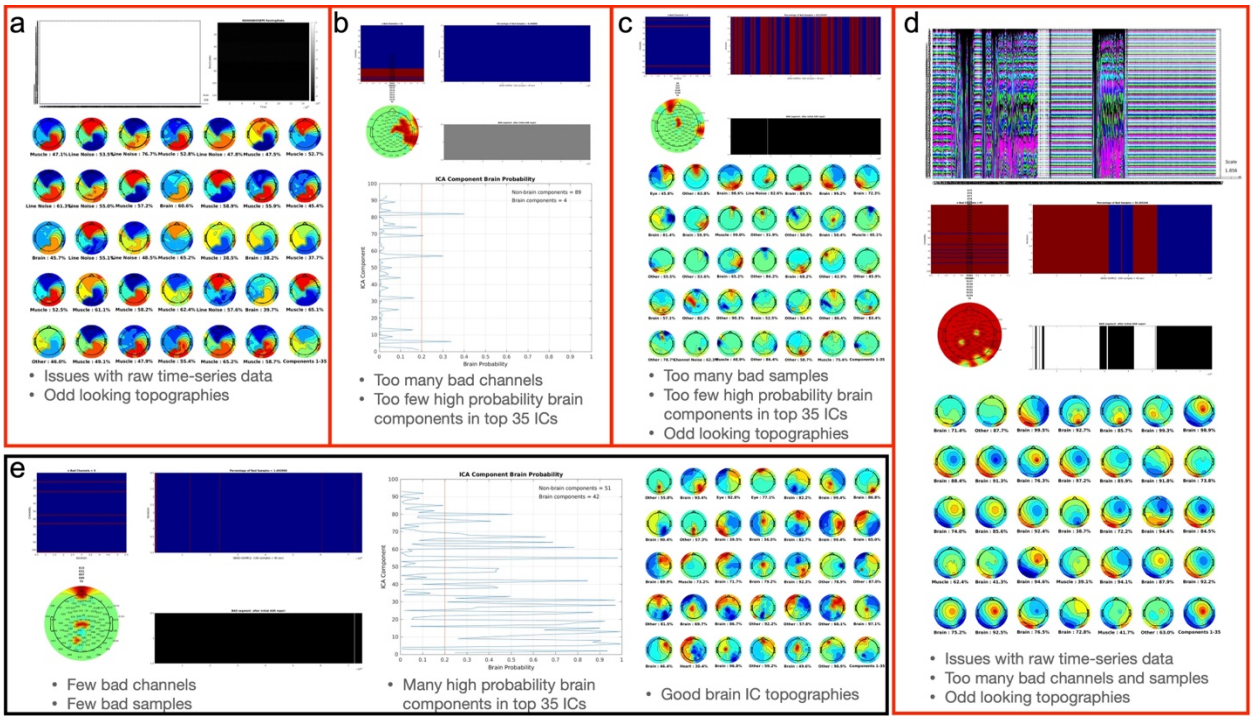

Supplementary Figure 4: Examples of issues flagged up in data quality control analysis that warranted exclusion (A-D) or inclusion of data into further downstream analysis. *Panels A-D show different examples of issues identified in data quality inspection at different step of the preprocessing pipeline. Panel E shows an example of a participant with relatively clean data and which was included in further downstream analysis.*

Supplementary Table Legends

Supplementary Table 1*: This table provides p-values from the SigClust analysis for eyes open and closed (rows) and training and validation sets (columns).*

Supplementary Table 2*: Statistics comparing individuals within autism E:I neurosubtypes that are consistent or inconsistent across resting state eyes open versus closed conditions.*

Supplementary Table 3*: Statistics per each electrode for main effects of subtype, age, and the subtype*age interaction, and also pair-wise autism subtype vs TD comparisons.*

Supplementary Table 4*: Statistics per each principal component for main effects of subtype, age, and the subtype*age interaction, pair-wise autism subtype vs TD comparisons, and effect sizes per each block of eyes open and closed conditions.*

Supplementary Table 5*: Descriptive statistics per each demographic or behavioral variable are shown in the table at the top. Directly below the descriptive statistics table are inferential statistics for a model testing for a between-group difference between TD, A1, and A2 (e.g., F-statistics, p-values, FDR). Below this table are further inferential statistical results for follow-up pair-wise comparisons between all groups are reported (e.g., t-statistics, p-values, FDR, Cohen's d). analyzing main effects of subtype, age, and the subtype*age interaction, pair-wise autism subtype vs TD comparisons, and effect sizes per each block of eyes open and closed conditions.*